Cryogenic laser operation of a “mixed” Yb:LuYAG garnet crystal

Sami Slimi, Venkatesan Jambunathan, Mingyan Pan, Yicheng Wang, Weidong Chen, Pavel Loiko, Rosa Maria Solé, Magdalena Aguiló, Francesc Díaz, Martin Smrz, et al.

Applied Physics B (2023) 129:57
https://doi.org/10.1007/s00340-023-07999-9

Applied Physics B
Lasers and Optics

RESEARCH

Cryogenic laser operation of a "mixed" Yb:LuYAG garnet crystal

Sami Slimi[1] · Venkatesan Jambunathan[2] · Mingyan Pan[3] · Yicheng Wang[4] · Weidong Chen[5] · Pavel Loiko[6] · Rosa Maria Solé[1] · Magdalena Aguiló[1] · Francesc Díaz[1] · Martin Smrz[2] · Tomas Mocek[2] · Xavier Mateos[1,7]

Received: 29 November 2022 / Accepted: 7 March 2023 / Published online: 25 March 2023

Abstract
We report on the continuous-wave and passively Q-switched operation of a compositionally "mixed" heavily doped 16.6 at.% Yb:$(Y,Lu)_3Al_5O_{12}$ garnet crystal at cryogenic temperatures (100–200 K), pumped by a volume Bragg grating stabilized diode laser emitting at 969 nm. At 140 K, in the continuous-wave regime, a maximum output power of 10.65 W was achieved at ~ 1029 nm with a slope efficiency of 56% (versus the incident pump power), a laser threshold of 1.05 W and excellent beam quality. Using Cr^{4+}:YAG as a saturable absorber, the passively Q-switched laser generated pulses with an energy/duration of 0.15 mJ/201 ns, respectively, at a repetition rate of 39.7 kHz, corresponding to a peak power of 0.39 kW.

1 Introduction

Operation of any diode-pumped solid-state laser (DPSSL) is associated with a deposition of heat in the laser medium. The heat loading leads to thermal lensing, depolarization loss and even laser ceasing due to a cavity instability or crystal fracture [1]. Ytterbium ions (Yb^{3+}), featuring a simple energy-level scheme, benefit from an in-band pumping scheme leading to a high slope efficiency and weak fractional heat loading (as compared to Nd^{3+} ones). This determines the prospects of Yb^{3+}-doped materials for the development of high-power DPSSLs emitting around 1 µm. Yb^{3+} ions can be efficiently pumped by commercial high-power fiber-coupled InGaAs diode lasers at ~ 976 nm [2]. They also provide a relatively long lifetime of the upper laser level ($^2F_{5/2}$), improving the energy storage capabilities for passively Q-switched operation [3]. Despite their intrinsically weak heat loading, Yb-based DPSSLs suffer from thermal effects, especially at moderate to high pump powers.

One solution to alleviate the thermal effects is to cool the laser crystal down to cryogenic temperatures [4]. There are several effects of such cooling [4–6]: (i) the thermal properties of the material improve, i.e., the thermal conductivity increases and thermal expansion and dn/dT coefficients drop, altogether contributing to weaker thermal lensing; (ii) the absorption and stimulated-emission cross sections of the active ions increase leading to higher gain; (iii) the thermal population of the terminal laser level for quasi-three-level gain media notably decreases, thus eliminating the reabsorption loss and reducing the laser threshold; (iv) the lifetime of the upper laser level also increases. In terms of spectroscopic properties, one drawback of the cryogenic cooling is the reduction of the absorption bandwidth. This challenge can be overcome by using volume Bragg grating stabilized diode lasers or employing gain media with inhomogeneous spectral broadening of absorption bands, i.e., crystals with a structure and/or compositional disorder.

Cubic yttrium and lutetium aluminum garnets, $Y_3Al_5O_{12}$ (YAG) and $Lu_3Al_5O_{12}$ (LuAG) [7] are well-known laser host

✉ Xavier Mateos
xavier.mateos@urv.cat

1 Universitat Rovira i Virgili (URV), Física i Cristal·lografia de Materials (FiCMA), Campus Sescelades 1, 43007 Tarragona, Spain

2 HiLASE Centre, Institute of Physics of the Czech Academy of Sciences, Za Radnicí 828, 252 41 Dolní Břežany, Czech Republic

3 Key Laboratory of Materials for High Power Laser, Shanghai Institute of Optics and Fine Mechanics, Chinese Academy of Sciences, Shanghai 201800, China

4 Photonics and Ultrafast Laser Science, Ruhr Universität Bochum, Universitätsstrasse 150, 44801 Bochum, Germany

5 Fujian Institute of Research On the Structure of Matter, Chinese Academy of Sciences, Fuzhou 350002, Fujian, China

6 Centre de Recherche sur les Ions, les Matériaux et la Photonique (CIMAP), UMR 6252 CEA-CNRS-ENSICAEN, Université de Caen Normandie, 6 Boulevard Maréchal Juin, 14050 Caen Cedex 4, France

7 Serra Húnter Fellow, Catalonia, Spain

crystals for Yb^{3+} doping. Due to the closeness of the ionic radii and weights of the host-forming (Lu^{3+}) and dopant (Yb^{3+}) cations, the LuAG crystal features much weaker dependence of its thermal conductivity on the Yb^{3+} doping level, which is essential for high-power DPSSL development [8–10]. Yb^{3+} ions in LuAG also offer somewhat better spectroscopic properties, namely, slightly broader ZPL in absorption at 969 nm, higher stimulated-emission cross section at ~ 1030 nm and slightly longer luminescence lifetime (as compared to Yb:YAG crystals) [7]. The growth of LuAG crystals is more complicated due to their higher solidification point and higher price of the Lu_2O_3 reagent [11].

As a result, "mixed" (solid-solution) crystals $Yb:(Y_{1-x}Lu_x)_3Al_5O_{12}$ or shortly Yb:LuYAG were suggested to combine the advantages of both parent compounds [12]. In such crystals, the regular garnet structure is distorted by replacing part of the Y^{3+} cations by Lu^{3+} ones. One can also expect additional inhomogeneous spectral broadening of the spectral bands of Yb^{3+} ions in such compounds. This could be particularly relevant for cryogenic lasers. Kuwano et al. reported on the growth of LuYAG crystals with different Lu^{3+} contents and their properties [11]. It was shown that such "mixed" crystals exhibit good thermo-physical properties and, because of the use of only partial substitution of Y^{3+} by Lu^{3+}, their growth is simplified as compared to that of LuAG. Continuous-wave laser operation of Yb:LuYAG crystals and transparent ceramics was studied [13–15].

There exist multiple studies on diode-pumped cryogenic laser operation of Yb:YAG [16–19] and only a few concerning Yb:LuAG [20], and both continuous-wave and passively Q-switched operation regimes have been explored. David et al. reported on a cryogenic (140 K) Yb:LuAG laser pumped by a volume Bragg grating stabilized laser diode delivering 10.5 W at 1030 nm with a slope efficiency of 48.6%, showing a significant improvement over output performance achieved at elevated temperatures.

In the present work, we aimed to study the laser performance of cryogenically cooled diode-pumped "mixed" Yb:LuYAG garnet crystals in the continuous-wave and passively Q-switched operation regimes.

2 Laser setup

As a laser gain medium, we have used a heavily Yb^{3+}-doped compositionally "mixed" $(Y,Lu)_3Al_5O_{12}$ garnet. A single crystal was grown by the Czochralski method using a [111] oriented seed in an Ar atmosphere and an induction heating system. The crystal was further annealed in air at 1400 °C for 12 h to remove the residual stresses and color centers causing crystal coloration. The annealed crystal was colorless. According to the ICP-AES analysis, the actual crystal composition was $(Y_{0.601}Lu_{0.233}Yb_{0.166})_3Al_5O_{12}$, corresponding to a doping level of 16.6 at.% Yb^{3+} (ion density: $N_{Yb} = 22.6 \times 10^{20}$ at/cm^3). A rectangular laser element was cut from the annealed crystal having an aperture of 4.0×4.0 mm^2 and a thickness of 2.0 mm. Both its faces were polished to laser-grade quality with good parallelism and left uncoated.

Figure 1 illustrates the schematic diagram of the cryogenic laser setup. An L-shaped cavity was formed by a concave rear mirror M1 coated for high reflection (HR) at 1030 nm (radius of curvature, RoC = − 300 mm), a plane dichroic bending mirror M2 coated for HR at 1020–1200 nm and high transmission (HT) at 900–980 nm, an antireflection (AR, at 1030 nm) coated plano-convex lens (L3) having a focal length of 150 mm and a series of plane output couplers (M3) with a transmission T_{OC} in the range of 10%, 20%, 30%, 40% and 50% in the spectral range of 1020–1070 nm.

The uncoated laser element was pumped by means of a volume Bragg grating (VBG) stabilized fiber-coupled diode laser (numerical aperture, N.A. = 0.22, fiber core diameter: 105 µm) emitting up to 60 W of unpolarized output at 969 nm with a spectral bandwidth (FWHM) of 0.4 nm. The pump thus addressed the absorption zero-phonon (ZPL) line of Yb^{3+} ions. The pump beam was collimated and focused into the laser element by two AR-coated achromatic lenses, L1 and L2 (1:2.5 reimaging ratio, focal lengths: $f = 100$ mm and 250 mm, respectively) resulting in a pump spot diameter of ~ 262 µm.

The laser performance was studied at several temperatures of the laser element. The crystal mounted inside a vacuum chamber was placed between the M2 folding mirror and the L3 intracavity lens at normal incidence. The crystal was wrapped into indium foil and mounted in a copper holder being conduction cooled. To avoid condensation at the sample surfaces upon cooling, the chamber was maintained at a pressure of 10^{-5} mbar. The cryogenic temperatures of the active medium were achieved by a closed-cycle helium cryostat (CH-204, JANIS), which provided a maximum cooling

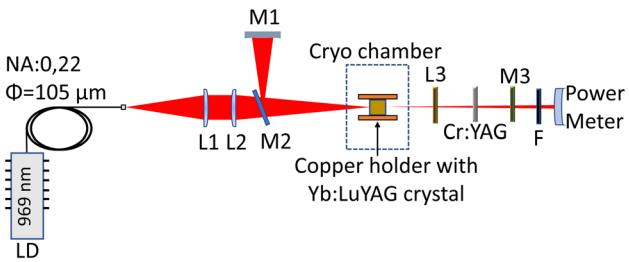

Fig. 1 Schematic of the experimental setup for studying the cryogenic laser performance of a 16.6 at.% Yb:LuYAG crystal. *LD* VBG-stabilized laser diode, *L1 and L2* a pair of achromatic lenses, reimaging ratio: 1:2.5, *M1* rear mirror, *M2* dichroic mirror, *L3* AR-coated intracavity lens, $f = 150$ mm, *M3* output coupler, *Cr:YAG* saturable absorber, *F* long-pass filter

power of 13.5 W at 100 K. A Lake Shore temperature controller (DT 670) was used to monitor and maintain the sample temperature, which included a silicon diode sensor and a 50 Ω heater.

The cavity was optimized for maximum output power by adjusting the separations between the optical elements. The measured optimum total geometrical cavity length was 755 mm, which included 301 mm between the M1 rear mirror and the input face of the crystal, 153 mm from its output face to the L3 intracavity lens, and 301 mm from L3 to the M3 output coupler. For passive Q-switching experiments, a saturable absorber (SA) was placed at 200 mm away from the L3 intracavity lens. Using the ABCD-matrix formalism, the mode diameters in the crystal and the SA were calculated to be ~ 220 and ~ 870 μm, respectively. The output power of the laser was measured using a thermal power sensor (S314 C, Thorlabs) and the measurement uncertainty was around ± 3% @ 1064 nm. The laser output was separated from the residual pump using a long-pass filter (FEL1000, Thorlabs) with a cut-off wavelength of 1000 nm and the transmission was around 84% @ 1030 nm.

To characterize passively Q-switched pulses, an ultrafast Si photodiode with a bandwidth of 6 GHz and a rise time of < 500 ps (UPD-500-UP, Alphalas) was used. The pulses were detected and recorded using a digital oscilloscope (Teledyne Lecroy Wavesurfer) with a bandwidth of 600 MHz and a sampling rate of 10 GS/s. The spectra of laser emission from the cryogenic laser were measured using an Ocean Optics compact spectrometer (model USB 2000+) with a spectral resolution of 0.3 nm.

3 Results and discussion

3.1 Cryogenic continuous-wave Yb:LuYAG laser

First, the input–output characteristics of the CW cryogenic diode-pumped Yb:LuYAG laser were studied by fixing the output coupler transmission ($T_{OC} = 30\%$) and varying the crystal temperature in the range of 100–200 K with a step of 20 K, as shown in Fig. 2a. The best output characteristics were achieved for an intermediate temperature of 140 K: the laser generated a maximum output power of 8.88 W at 1028.9 nm with a slope efficiency η of 51% (vs. the incident pump power) and a laser threshold of 0.98 W. The optical efficiency at the highest incident pump power of 18.21 W amounted to 51%. For smaller crystal temperatures, the laser performance deteriorated due to the rapidly decreasing pump absorption (see below). When increasing the temperature from the optimum one up to 200 K, the maximum output power decreased (down to 5.93 W), the slope efficiency also decreased (to 38%) and the laser threshold raised (to 2.45 W), as shown in Fig. 2b. For the crystal temperatures in the range of 120–200 K, the output dependences were linear for the studied range of pump powers. Figure 2c shows the temperature dependence of the laser wavelength. With increase in the temperature from 100 to 200 K, it experienced a slight monotonous red-shift from 1028.7 to 1029.3 nm.

After selecting the optimum crystal temperature (140 K), the effect of the output coupler transmission on the laser performance was studied, see Fig. 3a. For 40% OC, the laser generated 10.65 W at 1029 nm with a slope efficiency η of 56% and a laser threshold of 1.05 W. With reducing the output coupling transmission, the laser performance progressively deteriorated: the output power and the slope efficiency decreased (down to 3.94 W and $\eta = 27\%$ for 10% OC). In addition, thermal rollover was observed for $T_{OC} = 10\%$ and 20%. It appeared at smaller pump powers when reducing the output coupling probably due to higher intracavity laser intensity. The laser threshold monotonously increased with the output coupling, from 1.05 to 1.43 W. The laser spectra were weakly dependent on T_{OC} and the emission was observed at 1028 nm, Fig. 3b. The laser linewidth was about 1 nm.

The pump absorption in the crystal was measured under non-lasing conditions at the threshold pump power assuming a single pass of the pump radiation. The calculation was done by taking into consideration the Fresnel losses at the uncoated crystal surface (assuming a refractive index n of 1.818). The pump absorption efficiency was about 72% at 140–200 K and below 140 K, it notably dropped (to 47% at 120 K and 18% at 100 K). This decrease in absorption was due to the blue-shift and narrowing of the absorption ZPL of Yb^{3+} ions in the garnet crystals. A similar behavior was previously observed for the parent Yb:YAG and Yb:LuAG garnet crystals at the temperatures below 140 K [20, 21]. Based on the determined pump absorption efficiency, we also plotted the output dependence of the laser with respect to the absorbed pump power, as shown in Fig. 4a. At 140 K, using 30% OC, the corresponding slope efficiency amounted to 71%. Figure 4b shows a typical far-field beam profile measured at the maximum output power corresponding to the fundamental transverse mode. A perfectly circular beam with a Gaussian intensity distribution was obtained confirming the excellent thermal management on the gain media by cryogenic cooling. Based on the CW laser results, the optimum temperature (140 K) and the output coupler transmission (40%) were chosen for further passively Q-switched laser experiments.

3.2 Passively Q-switched cryogenic Yb:LuYAG laser

Passive Q-switching of the cryogenic Yb:LuYAG laser was realized using AR-coated Cr^{4+}:YAG SAs with two different initial transmissions at the laser wavelength T_{SA} of 85% and 95%. The input–output dependences for the

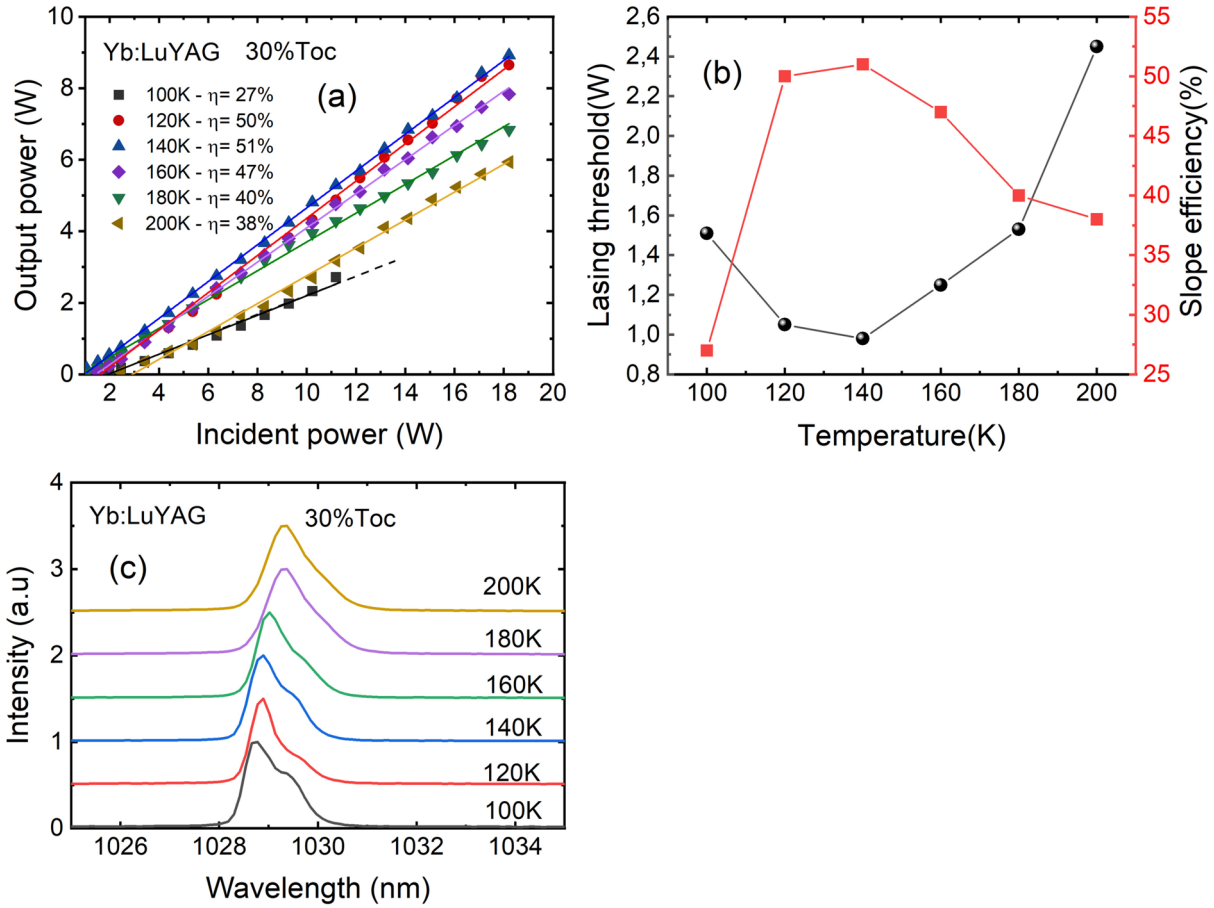

Fig. 2 CW diode-pumped cryogenic Yb:LuYAG laser: **a** input–output dependences for various crystal temperatures at a fixed T_{OC} of 30%, η-slope efficiency; **b** slope efficiency (red squares) and laser threshold (blue circles) as a function of the crystal temperature from 100 to 200 K; **c** laser emission measured at different temperatures for $T_{OC}=30\%$

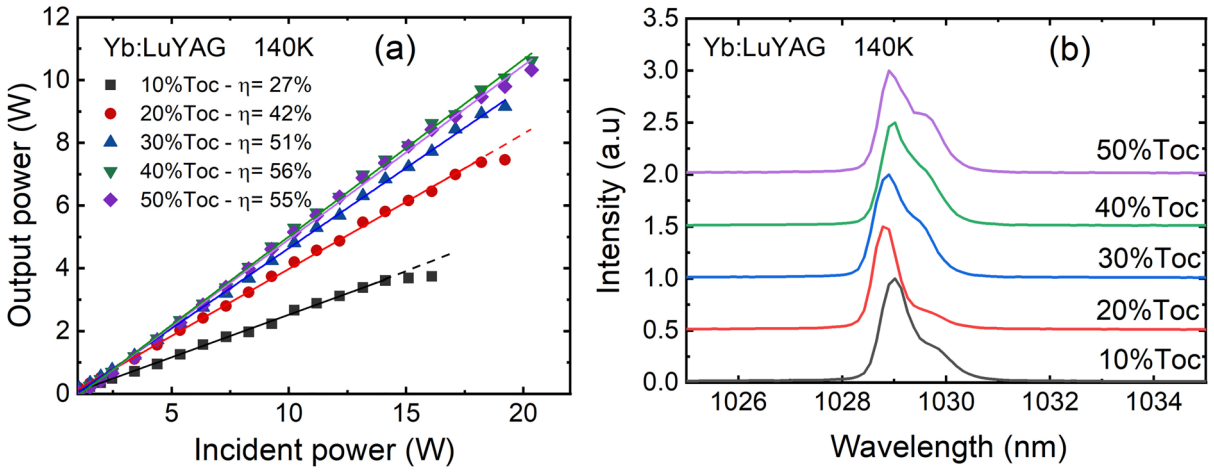

Fig. 3 Effect of the output coupler transmission on the output performance of the CW diode-pumped cryogenic Yb:LuYAG laser: **a** input–output dependences, η-slope efficiency; **b** typical spectra of laser emission. Crystal temperature: 140 K

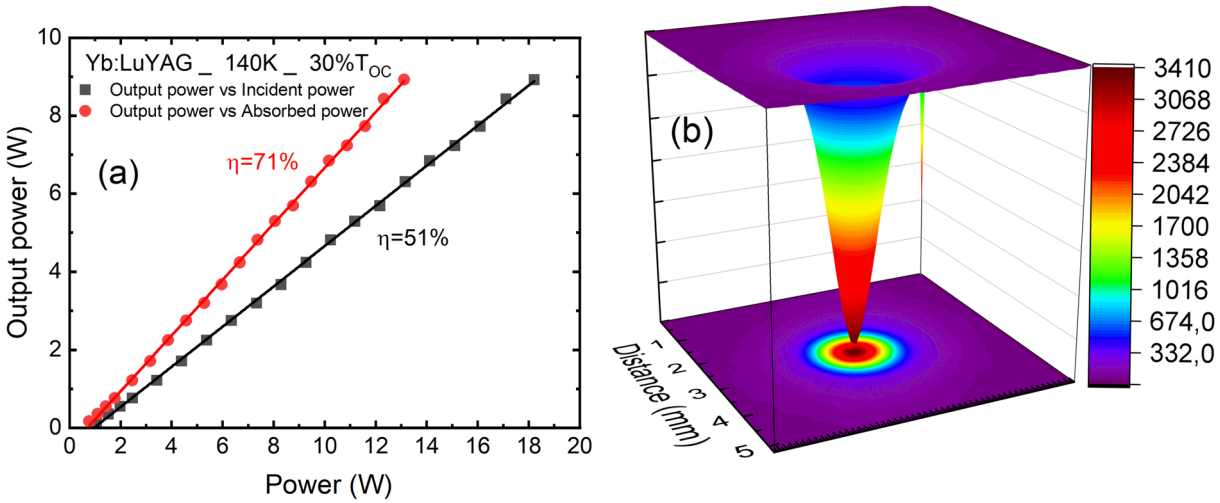

Fig. 4 CW diode-pumped cryogenic Yb:LuYAG laser: **a** output power versus the incident and absorbed pump powers at 140 K using 30% OC; **b** a typical far-field beam profile captured at the maximum output power

passively *Q*-switched Yb:LuYAG laser operated at 140 K are shown in Fig. 5a. The average output power increased with the initial transmission of the SA. A maximum average output power of 8.28 W corresponding to a slope efficiency of 49% was achieved for the SA with T_{SA} of 95%. For the SA with a higher modulation depth ($T_{SA}=85\%$), the laser generated 6.05 W with a lower slope efficiency of 39%. The laser operated on the fundamental transverse mode, see the far-field beam profile depicted at the inset of Fig. 5a. The pulse duration $\Delta\tau$ (FWHM) and the pulse repetition rate (PRR) of the passively Q-switched Yb:LuYAG laser are shown in Fig. 5b. The PRR increased almost linearly with the incident pump power, from 44 to 105 kHz ($T_{SA}=95\%$) and from 11 to 39.7 kHz ($T_{SA}=85\%$.) Smaller PRR values for the SA with a higher modulation depth are due to higher pulse energies. The pulse duration decreased with the incident pump power just above the laser threshold, and then showed a weak dependence on the pump level. The shortest pulse durations were 201 ns and 346 ns, measured using the SAs with $T_{SA}=85\%$ and 95%, respectively. The corresponding oscilloscope traces of the shortest single Q-switched pulses are shown in Fig. 6a. The calculated pulse energy, $E_{out}=P_{out}/\mathrm{PRR}$, and the peak power, $P_{peak}=E_{out}/\Delta\tau$, are shown in Fig. 6b. The pulse energy

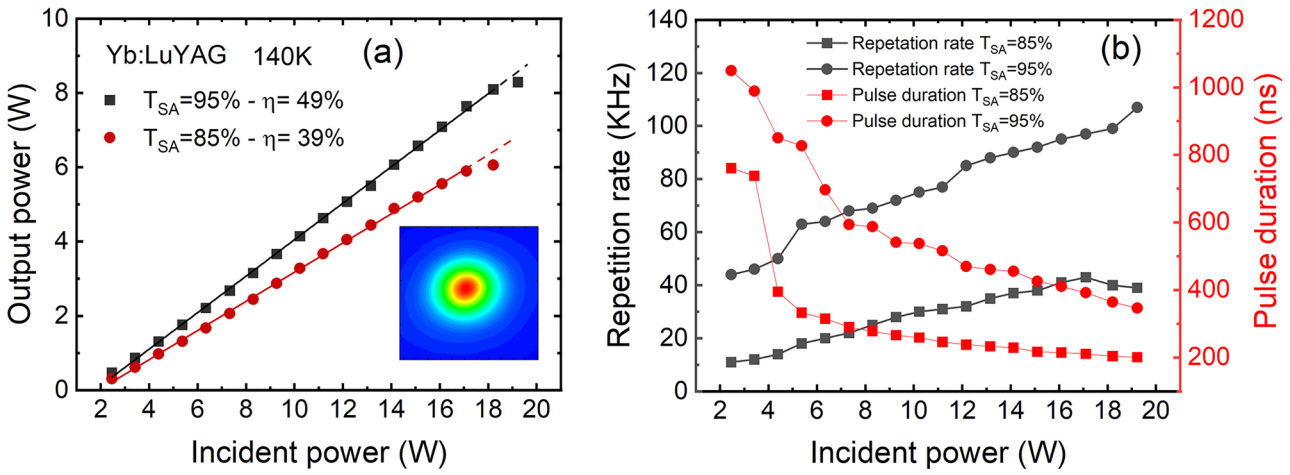

Fig. 5 Passively Q-switched diode-pumped cryogenic Yb:LuYAG laser: **a** average output power versus incident pump power for two different initial transmissions of the Cr^{4+}:YAG SA ($T_{SA}=85$ and 95%). The inset shows the intensity profile of the laser beam recorded at the maximum incident power with $T_{SA}=95\%$; **b** pulse repetition rate and pulse duration (FWHM) versus incident pump power. Crystal temperature: 140 K

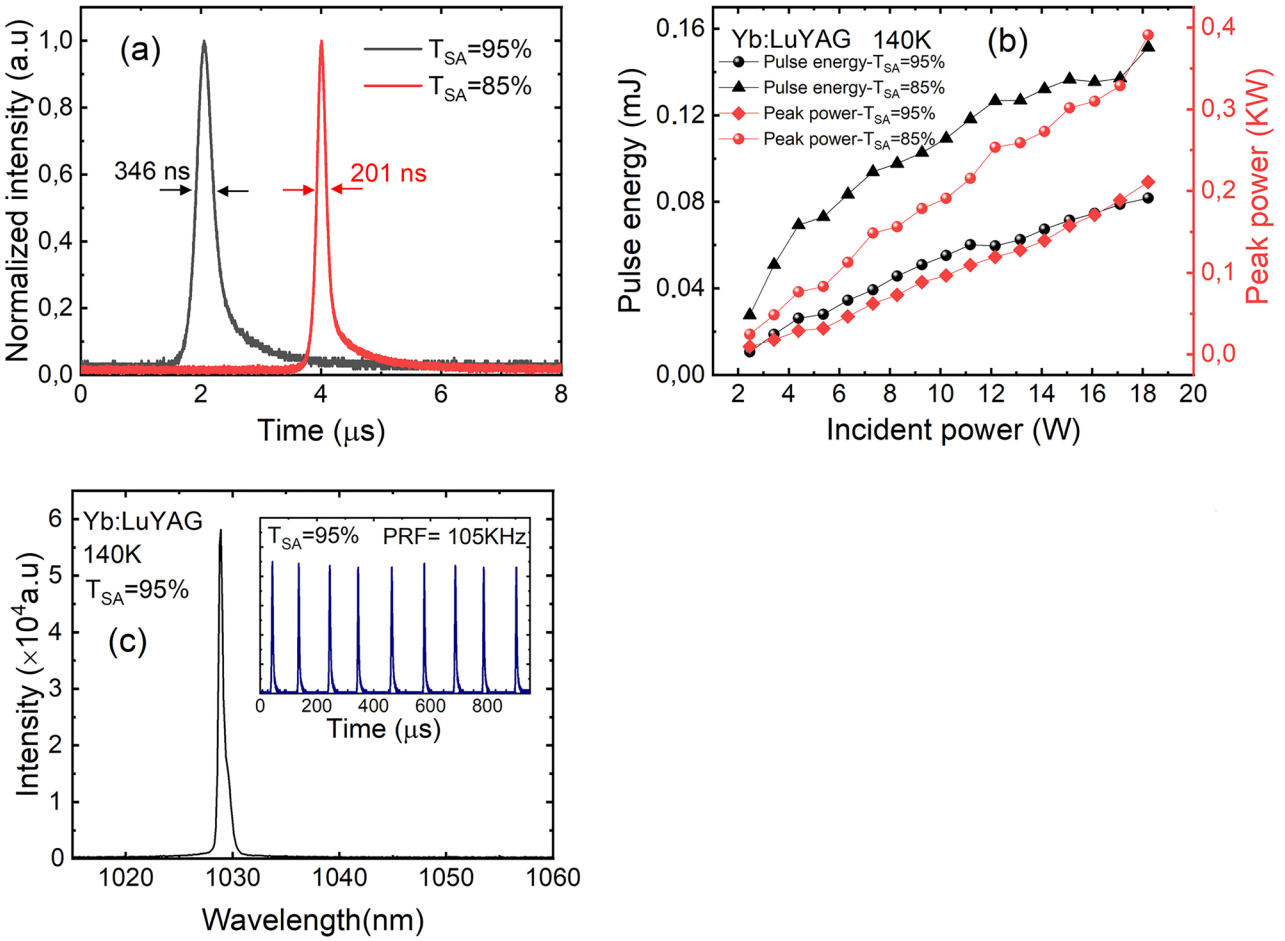

Fig. 6 Passively Q-switched diode-pumped cryogenic Yb:LuYAG laser: **a** oscilloscope traces of the shortest Q-switched pulses recorded at the maximum incident pump power for various T_{SA}; **b** pulse energy and peak power; **c** a typical laser spectrum, inset shows an oscilloscope trace of the corresponding pulse train, $T_{SA}=95\%$. Crystal temperature: 140 K

gradually increased with the pump power. The maximum pulse energy of 0.15 mJ was achieved when using the SA with $T_{SA}=85\%$. The corresponding maximum peak power was 0.39 kW. The output characteristics of the passively Q-switched laser are summarized in Table 1. The laser wavelength was centered at 1028.9 nm, Fig. 6c. Further shortening of Q-switched pulses is expected by increasing the modulation depth of Cr^{4+}:YAG SAs or by shortening the cavity length to reduce the cavity roundtrip time [22].

4 Conclusion

To conclude, the ytterbium-doped "mixed" (yttrium–lutetium) aluminum garnet crystal is attractive for the development of high-power diode-pumped cryogenic lasers emitting at ~ 1030 nm. In the continuous-wave regime, pumping by a VBG-stabilized laser diode at 969 nm, a maximum output power of 10.65 W was achieved at 1029 nm with a slope efficiency of 56% with respect to the incident pump power, at the crystal temperature of 140 K. The optimum

Table 1 Output characteristics of the diode-pumped cryogenic Yb:LuYAG laser passively Q-switched by Cr^{4+}:YAG saturable absorbers

T_{SA} (%)	Average output power (W)	Slope efficiency (%)	Pulse duration (ns)	Pulse repetition rate (kHz)	Pulse energy (mJ)	Peak power (kW)
85	6.05	39	201	39.7	0.15	0.39
95	8.28	49	346	105	0.081	0.21

operation temperature and the output performance of the "mixed" Yb:LuYAG crystal were similar to those found for Yb:LuAG. However, the former compound benefits from the simplified and more cost-efficient growth procedure. By employing Cr^{4+}:YAG based saturable absorbers, for the passively Q-switched cryogenic laser, the best pulse characteristics (energy/duration) were 0.15 mJ/201 ns at a repetition rate of 39.7 kHz. Future work will focus on active Q-switching using KD*P or BBO based Pockels cells to increase the pulse energy. Other cavity designs will also be studied.

Acknowledgements This research article has been possible with the support of the Secretaria d'Universitats i Recerca del Departament d'Empresa i Coneixement de la Generalitat de Catalunya, the European Union (UE), and the European Social Fund (ESF) (2021 FI_B1 00170). Grant PID2019-108543RB-I00 was funded by MCIN/AEI/10.13 039/501100011033. This work was co-financed by the European Regional Development Fund and the state budget of the Czech Republic (project HiLASE CoE: Grant No. CZ.02.1.01/0.0/0.0/15_006/0000674) and by the European Union's Horizon 2020 research and innovation program under Grant Agreement No. 739573.

Author contributions Sami Slimi: Conceptualization, Investigation, Methodology, Writing & editing. - Original Draft.Venkatesan Jambunathan: Conceptualization, Investigation, Methodology, Writing & editing. - Original Draft.Mingyan Pan: InvestigationYicheng Wang: InvestigationWeidong Chen: Investigation, Conceptualization.Pavel Loiko: Conceptualization, Writing - Review & Editing.Rosa Maria Solé: Conceptualization, Writing - Review & Editing.Magdalena Aguiló: Funding acquisition, Review & Editing.Francesc Díaz: Funding acquisition, Review & Editing.Martin Smrz: Supervision, Resources, Review & Editing.Tomas Mocek: Funding acquisition, Review & Editing.Xavier Mateos: Writing - Review & Editing, Funding acquisition, Supervision.

Funding Open access funding provided by Universitat Rovira i Virgili.

Data availability The data that support the findings of this study are available from the corresponding author, [X.M.], upon reasonable request.

Declarations

Competing interests The authors declare no competing interests.

References

1. S. Chénais, F. Druon, S. Forget, F. Balembois, P. Georges, Prog. Quantum Electron. **30**, 89 (2006)
2. H.W. Bruesselbach, D.S. Sumida, R.A. Reeder, R.W. Byren, IEEE J. Sel. Top. Quantum Electron. **3**, 105 (1997)
3. P. Deng, J. Xu, J. Dong, Y. Liu, X. Xie, Y. Zhang, W. Chen, Appl. Opt. **40**(24), 4303–4307 (2001)
4. T.Y. Fan, D.J. Ripin, R.L. Aggarwal, J.R. Ochoa, B. Chann, M. Tilleman, J. Spitzberg, IEEE J. Sel. Top. Quantum Electron. **13**, 448 (2007)
5. R.L. Aggarwal, D.J. Ripin, J.R. Ochoa, T.Y. Fan, J. Appl. Phys. **98**, 103514 (2005)
6. D.C. Brown, IEEE J. Sel. Top. Quantum Electron. **11**, 587 (2005)
7. H. Canibano, A. Ródenas, D. Jaque, A.G. Petrosyan, G. Boulon, Y. Guyot, A. Brenier, A. Eganyan, JOSA B **23**(4), 676–683 (2006)
8. H. Nakao, K. Ueda, A. Shirakawa, H. Yagi, T. Yanagitani, Opt. Express **20**(14), 15385–15391 (2012)
9. Y. Fu, J. Li, C. Wang, T. Xie, W. Li, L. Wu, Y. Pan, J. Alloys Compd. **664**, 595 (2016)
10. S.T. Fredrich-Thornton, K. Beil, R. Peters, F. Tellkamp, C. Kränkel, K. Petermann, G. Huber, Opt. Express **18**(20), 20712–20722 (2010)
11. Y. Kuwano, K. Suda, N. Ishizawa, T. Yamada, J. Cryst. Growth **260**, 159 (2004)
12. S. Cheng, X. Xu, D. Li, D. Zhou, F. Wu, Z. Zhao, J. Xu, Opt. Mater. (Amst). **33**, 112 (2010)
13. V.V. Balashov, L.Y. Zakharov, A.V. Inyushkin, A.Y. Kanaev, A.B. Kozlov, S.M. Kozlova, A.L. Koromyslov, K.V. Lopukhin, V.A. Luzanov, K.S. Pervakov, I.M. Tupitsyn, D.A. Chernodoubov, E.A. Cheshev, Ceram. Int. **48**, 6294 (2022)
14. A. Pirri, G. Toci, J. Li, T. Xie, Y. Pan, V. Babin, A. Beitlerova, M. Nikl, M. Vannini, Opt. Mater. (Amst). **73**, 312 (2017)
15. S. Lv, C. Gao, Z. Tian, X. Su, G. Wang, G. Zhu, B. Wang, S. Kumar, X. Xu, H. Yu, X. Lin, J. Xu, B. Zhang, Opt. Commun. **478**, 126356 (2021)
16. S. Tokita, J. Kawanaka, M. Fujita, T. Kawashima, Y. Izawa, Jpn. J Appl. Phys. Part 2 Lett. **44**, L1529 (2005)
17. J.G. Manni, J.D. Hybl, D. Rand, D.J. Ripin, J.R. Ochoa, T.Y. Fan, IEEE J. Quantum Electron. **46**, 95 (2010)
18. T.Y. Fan, R.L. Aggarwal, J.R. Ochoa, D.J. Ripin, Opt. Lett. **29**(18), 2154–2156 (2004)
19. J. Kawanaka, Y. Takeuchi, A. Yoshida, S.J. Pearce, R. Yasuhara, T. Kawashima, H. Kan, Laser Phys. **20**, 1079 (2010)
20. S. Paul David, V. Jambunathan, F. Yue, A. Lucianetti, T. Mocek, Opt. Laser Technol. **135**, 106720 (2021)
21. V. Jambunathan, L. Horackova, P. Navratil, A. Lucianetti, T. Mocek, IEEE Photonics Technol. Lett. **28**, 1328 (2016)
22. P. Navratil, V. Jambunathan, L. Horackova, A. Lucianetti, T. Mocek, **9726**, 287 (2016). https://doi.org/10.1117/12.2210960